NUMERICAL MODELLING OF PITCHING WINGS FOR GUST MITIGATION

Weixing Yuan[1], Alanna Wall[1], Xiaoyang Zhang[2], and Dominique Poirel[2]

[1]National Research Council (NRC) Canada, Ottawa, Ontario, K1A 0R6, Canada
[2]Royal Military College of Canada (RMC), Kingston, Ontario, K7K 7B4, Canada

Abstract

Urban environments are aerodynamically challenging for unmanned air vehicles (UAVs) because of complex flow structures and high levels of turbulence encountered around buildings. Therefore, studies have started focusing on the effects that gusting has on UAV aerodynamic stability and control. This study develops gust modelling capabilities towards understanding the aerodynamic response and more specifically gust mitigation strategies for UAVs operating in gusty urban environments. In particular, a radial basis function is applied to a modified split-velocity method for the numerical modelling of pitching wings for gust mitigation.

Keywords: Gust modelling, gust mitigation, pitching wings, UAV

1. Introduction

Unmanned aerial vehicles (UAVs) have ever-increasing requirements in both civilian and military settings for a wide range of applications and missions. There is a demand for UAVs to fly in difficult weather conditions in the presence of obstacles and close to populated areas. Like manned aircraft, a key requirement for the development and validation of guidance and control algorithms for UAVs is an accurate model of the vehicle dynamic response to control inputs and disturbances. However, the modelling of UAV flight dynamics poses some additional challenges that are not present with manned vehicles [1]; for instance, flight dynamics are not easily modelled using analytical methods. A realistic understanding of the environmental issues associated with UAV operations in urban and mountainous environments will aid in successful deployment by alleviating the susceptibility of UAVs to wind gusts [2].

Many potential UAV missions involve flying at low altitudes and in urban or mountainous environments, where wind gusts are prevalent. A gust is defined as any velocity deviation in either magnitude or direction from a uniform, steady, unidirectional flowfield. While small wind gusts and atmospheric turbulence may be of minor significance to larger, heavier, higher-altitude UAVs, they can be devastating for the stability and control of smaller and lighter UAVs. The lower inertias of these vehicles result in higher natural frequencies of the vehicle dynamics and shorter vehicle response times [1]. The dynamic characteristics of small-scale vehicles are related to the dynamics of larger (manned scale) vehicles by Froude scaling. When Froude scaling is used, the natural frequency increases by a factor of two for a one-fourth scale vehicle. This dictates the need for higher bandwidth flight control systems, thus requiring higher bandwidth dynamic models for analysis [1].

Gusting aerodynamics affect the stability and control of aircraft flight. The governing equations of motion for aircraft are derived from Newton's second law. Traditionally, the flight dynamics equations can be linearized by using small disturbance theory. It is assumed that both the net force and net moment on the aircraft are zero. In the presence of a gust, the longitudinal and lateral motion equations are modeled in state space form as follows [2]:

$$\dot{\mathbf{x}} = \mathbf{A}\mathbf{x} + \mathbf{B}u + \mathbf{T}g, \tag{1}$$

where the $\mathbf{A}$ matrix consists of the aircraft stability derivatives and the $\mathbf{B}$ matrix consists of the control derivatives, $\mathbf{x}$ represents a vector of either longitudinal or lateral state variables, and u contains inputs capable of altering any of the variables contained in the above equation, such as elevator deflection δ_e or a change in thrust settings δ_t, aileron angle δ_a or rudder angle δ_r. $\mathbf{T}$ stands for the gust input matrix and g contains the components of the gust vector. If $\mathbf{B}u = \text{-}\mathbf{T}g$, one would eliminate the effect of the gust and thus the aircraft would behave as if flying through still air. In practice, gust alleviation is accomplished by choosing one or more variables to be controlled in some manner (held constant, eliminated, minimized, etc.) and designing an algorithm to achieve this goal. The accuracy of such methods depends to a large extent on the information available when developing the control algorithm, where results are likely to be better if matrix $\mathbf{A}$ is a good representation of the system, and as more feedback is designed into it.

Gust modelling plays an important role in both the design and operation of modern aircraft. Early analytical gust models focused on a discrete gust, that of a finite change in velocity occurring only once. Gusts were modeled as an additional component of the flow perpendicular or parallel to the oncoming flow, added vectorially to the freestream velocity. This change in the direction and magnitude of the velocity vector affected the lift generated by the wing in both a spatial and temporal sense, and thus the loads an aircraft encounters. In dynamic terms, the perpendicular (vertical or transverse) component of the gust acts as an external force, whereas the longitudinal (horizontal or in-plane) component acts as a parametric force [3]. In principle, the latter makes matrix $\mathbf{A}$ time-dependent, which can complicate the modelling and the solution significantly. In the gust control application mentioned above, it is assumed that the gust intensity is relatively small, such that the aircraft behaves linearly as modelled in Eq. (1).

To account for nonlinearities in the real world, high-order computational fluid dynamics (CFD) is increasingly applied to the gust response aerodynamics. Because it is difficult to impose arbitrary disturbances at curved boundaries, Lockard and Morris [4] introduced a gust source inside the computational domain to model the airfoil-gust interaction. They assumed that the gust is incompressible and vortical, and that only the momentum equations need to be modified. Golubev et al. [5] applied this gust model in viscous simulations of gust interaction with stationary and pitching wings. Singh and Baeder [6] proposed a field-velocity method that was applied by Sitaraman and Baeder [7] in simulating responses to a traveling gust. Further, Wales et al. [8] proposed a split-velocity method where the velocity components in the two-dimensional (2D) Euler equations are decomposed into a prescribed gust velocity and the remaining velocity components. Both the field- and split-velocity methods are velocity-prescribed methods, where the gust and any wing motion present are both known and prescribed at the grid points. The main difference between the field- and split-velocity approaches is that the split-velocity method contains source terms derived from the governing equations for gusting while they are neglected in the field-velocity method. The source term is needed to capture the full interaction between the wing body and the gust. A closer comparison shows that Lockard and Morris' approach can be seen as a simplified version of the split-velocity method, with a progressively simplified gust source term in the momentum equations while assuming that the gusts are incompressible and divergence free. More recently, the split-velocity method was applied to computational investigations of transverse gust encounters by Badrya et al. [9] and Biler et al. [10].

The long-term objective of the present study is to develop a capability in gust modelling to understand the aerodynamic and aeroelastic responses of UAVs to gusts and thus build aerodynamic models applicable to the mitigation and control of UAV-gust interactions. In this study, the split-velocity method, originally developed for compressible flows based on 2D Euler equations [8], is modified and further developed for incompressible flows and then applied to simulations of 3D aerodynamic responses to gusts, towards future aeroelastic applications. In the modified split-velocity method, the full velocity containing the gust component is used in the viscous terms, whereas the gust velocity was neglected in Refs. [9] and [10]. The present study further clarifies the necessity of not including the gust velocity in the space conservation law for simulations on moving grids for strict mass conservation, whereas the gust velocity was combined with the grid velocity in discretizing the space

conservation law in Refs. [6] and [7]. Furthermore, a mesh-morphing technology based on a radial basis function (RBF) was applied to include a wing pitch degree of freedom for mitigation of gust effects. Available computed results are presented in this paper to demonstrate the methodology development and its applications.

2. CFD Flow Solver

UAVs are produced in a wide range of shapes and sizes. Large-sized UAVs operate in Mach- and Reynolds-number regimes for which there is extensive aerodynamic experience and knowledge. It is with micro- to mid-sized UAVs operating at low Mach numbers (or in the incompressible flow regime) and lower Reynolds numbers that most of the current aerodynamic and propulsion challenges lie. As for the aerodynamics of these small UAVs, the designers must contend with transitioning and separating flows where the dominating flow structures are difficult to capture without resorting to higher-order turbulence models, thereby demanding increased computational requirements. These issues become even more acute when one or more components of the flight vehicle are in continuous relative motion, such as when the wing is oscillating, flapping, plunging, or rotating in real time.

The major problem in the prediction of incompressible or low-Mach-number flows, even without the added challenges involving moving boundaries, is the convergence of the static pressure in the flowfield. Since the fluid density is constant, a time-independent constraint must be imposed to couple the changes in the velocity field with the pressure field while satisfying the continuity equation. The concepts of numerical methods used for the simulations of unsteady incompressible flows under gust encounters were introduced in a previous study [11]. To aid readers' understanding, the modified split-velocity method is briefly described in this section, followed by an additional technical implementation of the RBF.

2.1 Conservation Laws

The principle of conservation of mass can be stated either with reference to a moving control volume (CV) or a volume fixed in space. For an arbitrarily shaped domain of a moving control volume V bounded by a closed surface A, the continuity equation is written as follows [12]:

$$\frac{d}{dt}\iiint_{V(t)} \rho dV + \iint_{A(t)} \rho(\vec{\mathbf{u}} - \vec{\mathbf{x}}_\tau) \cdot \vec{\mathbf{n}} dA = 0. \tag{2}$$

In this equation, ρ represents the fluid density, $\vec{\mathbf{u}}$ the fluid velocity, and $\vec{\mathbf{x}}_\tau$ the velocity of grid movement, respectively. $\vec{\mathbf{n}}$ is the unit vector orthogonal to the surface A.

The law of conservation of momentum is a restatement of Newton's second law of motion applied to a closed system; mass flows in and out of the system. For Newtonian fluids and assuming no body forces, the integral form of the momentum conservation equation is [12]:

$$\frac{d}{dt}\iiint_{V(t)} \rho\vec{\mathbf{u}} dV + \iint_{A(t)} \rho\vec{\mathbf{u}}(\vec{\mathbf{u}} - \vec{\mathbf{x}}_\tau) \cdot \vec{\mathbf{n}} dA = \iint_{A(t)} (-p\vec{\mathbf{I}} + \vec{\mathbf{T}}) \cdot \vec{\mathbf{n}} dA, \tag{3}$$

where p stands for pressure and $\vec{\mathbf{I}}$ is the unit tensor. The stress tensor $\vec{\mathbf{T}}$ can be written as

$$\vec{\mathbf{T}} = \frac{2}{3}\mu(\mathrm{div}\vec{\mathbf{u}})\vec{\mathbf{I}} + 2\mu\vec{\mathbf{D}}, \tag{4}$$

where μ is the fluid dynamic viscosity. The rate of strain (deformation) $\vec{\mathbf{D}}$ is defined as:

$$\vec{\mathbf{D}} = \frac{1}{2}\left[\text{grad}\vec{\mathbf{u}} + (\text{grad}\vec{\mathbf{u}})^T\right]. \tag{5}$$

In this study, the calculations were mainly performed on moving grid configurations. To avoid artificial mass sources generated by the grid velocity, a space conservation law given by

$$\frac{d}{dt}\iiint\limits_{V(t)} dV - \iint\limits_{A(t)} \vec{\mathbf{x}}_\tau \cdot \vec{\mathbf{n}}dA = 0 \tag{6}$$

was introduced to ensure a fully conservative property in the computations, as applied by Demirdžić and Perić [13].

2.2 Gust Modelling

To model the gust, the velocity vector of the flow is decomposed as follows [8]:

$$\vec{\mathbf{u}} = \vec{\tilde{\mathbf{u}}} + \vec{\mathbf{u}}_{\mathbf{g}}, \tag{7}$$

where $\vec{\mathbf{u}}_{\mathbf{g}}$ is the vector of the prescribed gust velocity. Separating the applied gust velocity $\vec{\mathbf{u}}_{\mathbf{g}}$ from the rest of the solution $\vec{\tilde{\mathbf{u}}}$, the mass and momentum conservation laws can be rewritten as

$$\frac{d}{dt}\iiint\limits_{V(t)} \rho dV + \iint\limits_{A(t)} \rho(\vec{\tilde{\mathbf{u}}} - \vec{\tilde{\mathbf{x}}}_\tau) \cdot \vec{\mathbf{n}}dA = 0, \tag{8}$$

$$\frac{d}{dt}\iiint\limits_{V(t)} \rho\vec{\tilde{\mathbf{u}}}dV + \iint\limits_{A(t)} \rho\vec{\tilde{\mathbf{u}}}(\vec{\tilde{\mathbf{u}}} - \vec{\tilde{\mathbf{x}}}_\tau) \cdot \vec{\mathbf{n}}dA + s_m(\vec{\mathbf{u}}_{\mathbf{g}}) = \iint\limits_{A(t)} (-p\vec{\mathbf{I}} + \vec{\mathbf{T}}) \cdot \vec{\mathbf{n}}dA, \tag{9}$$

where the gust velocity is added to the grid velocity as

$$\vec{\tilde{\mathbf{x}}}_\tau = \vec{\mathbf{x}}_\tau - \vec{\mathbf{u}}_{\mathbf{g}}, \tag{10}$$

and the gust source term is

$$s_m(\vec{\mathbf{u}}_{\mathbf{g}}) = \frac{d}{dt}\iiint\limits_{V(t)} \rho\vec{\mathbf{u}}_{\mathbf{g}}dV + \iint\limits_{A(t)} \rho\vec{\mathbf{u}}_{\mathbf{g}}(\vec{\tilde{\mathbf{u}}} - \vec{\tilde{\mathbf{x}}}_\tau) \cdot \vec{\mathbf{n}}dA. \tag{11}$$

For simulations on moving grids, the space conservation law in Eq. (6) must be fulfilled. It should be noted that the grid velocity $\vec{\mathbf{x}}_\tau$ does not contain the gust velocity $\vec{\mathbf{u}}_{\mathbf{g}}$ for geometric conservation, which is different from previous studies [6] and [7], where the modified grid velocity $\vec{\tilde{\mathbf{x}}}_\tau$ containing the gust velocity was used in the field-velocity method. Use of the correct grid velocity is important to avoid a mass source and thus ensure that the mass conservation law holds as the gust velocity is part of the total velocity of the flow. As a result, combining Eq. (6) with Eq. (2) ensures that the continuity equation of the full velocity for incompressible flows is satisfied,

$$\iint\limits_{A} \vec{\mathbf{u}} \cdot \vec{\mathbf{n}}dA = 0. \tag{12}$$

Also note that, different from previous research work [8], where the gust source term was used in a non-conservative differential form, the current integral form of Eq. (11) is in a conservative form, which allows consistent discretization as applied to other convective terms in the conservative form.

2.3 Morphing of CFD Mesh Deformation

For CFD applications, a mesh deformation algorithm is required to deform the flow mesh based on the boundary displacements due to the interaction with the flexible or moving structure. Since the spline approach is valid for both volume mesh smoothing and surface shape changes [14], the dynamic CFD mesh was updated using an RBF without successive calling of a grid generator. In this study, displacement interpolation using the RBFs was conducted for all nodes of the flow mesh.

An interpolation function for general spline problem was defined for the deformation w at the location (x, y, z), which is composed of a linear polynomial and a radial basis:

$$w(x, y, z) = a_0 + a_1 x + a_2 y + a_3 z + \sum_{i=1}^{N} K_i(x, y, z) F_i. \tag{13}$$

$$\sum_{i=1}^{N} F_i = 0; \quad \sum_{i=1}^{N} x_i F_i = 0; \quad \sum_{i=1}^{N} y_i F_i = 0; \quad \sum_{i=1}^{N} z_i F_i = 0. \tag{14}$$

The RBF $K_i(x, y, z)$ defines the radial interactions with the source points, and the polynomial corrector $a_0 + a_1 x + a_2 y + a_3 z$ guarantees compatibility for rigid modes. An RBF is a real-valued function whose value depends only on the distance from the origin (r), so that $K_i(x, y, z) = K(r_i)$ where $r_i^2 = (x - x_i)^2 + (y - y_i)^2 + (z - z_i)^2$.

$$
\begin{Bmatrix} 0 \\ 0 \\ 0 \\ 0 \\ w_1 \\ ... \\ w_N \end{Bmatrix}
=
\begin{bmatrix}
0 & 0 & 0 & 0 & 1 & ... & 1 \\
0 & 0 & 0 & 0 & x_1 & ... & x_N \\
0 & 0 & 0 & 0 & y_1 & ... & y_N \\
0 & 0 & 0 & 0 & z_1 & ... & z_N \\
1 & x_1 & y_1 & z_1 & 0 & ... & K_{1N} \\
... & ... & ... & ... & ... & ... & ... \\
1 & x_N & y_N & z_N & K_{N1} & ... & 0
\end{bmatrix}
\begin{Bmatrix} a_0 \\ a_1 \\ a_2 \\ a_3 \\ F_1 \\ ... \\ F_N \end{Bmatrix}
= [\mathbf{C}]
\begin{Bmatrix} a_0 \\ a_1 \\ a_2 \\ a_3 \\ F_1 \\ ... \\ F_N \end{Bmatrix}. \tag{15}
$$

Built on the known values at the source points, the matrix system can be defined and the inverse matrix $[\mathbf{C}]^{-1}$ can be used to calculate the coefficients F_i of the RBF and the coefficients a_{0-3} of the linear polynomial in Eq. (13). The matrix $[\mathbf{C}]^{-1}$ was pre-generated and stored at the beginning in the simulation. Several RBFs were implemented in the current RBF module. Based on experiences learned from applications related to computational aeroelasticity [15], the simple polyharmonic spline $K(r) = |r|$ was used in this study.

2.4 Numerical Method

The aforementioned governing Eqs. (6), (8) and (9) with split velocities were implemented in the in-house CFD code INSflow [16] that was developed for computing three-dimensional (3D) unsteady incompressible Navier-Stokes flows. INSflow has been used for numerous large-eddy simulations (LESs) and unsteady Reynolds-averaged Navier-Stokes (URANS) calculations of various flows. Recent numerical investigations on low-Reynolds-number aerodynamics, flapping-wing aerodynamics and laminar-separation flutter were reported in Refs. [17] – [19].

The integral form of the conservation laws of mass and momentum mentioned above was used in INSflow. A fully-implicit second-order temporal differencing scheme was used in the discretization, which made the algorithm stable for large time steps. The discretization of the convective and diffusive fluxes was carried out in a co-located variable arrangement using a finite-volume approach

that was second-order accurate in space. To ensure numerical stability, an upwind scheme was also implemented in addition to the second-order central differencing scheme, which could define a hybrid scheme. Since the code is an incompressible flow solver, the coupling of the pressure and velocity was handled employing the SIMPLE algorithm [20]. The continuity equation was transformed into a pressure-correction equation that had the same general form as the discretized momentum equations. The use of the co-located variable arrangement on non-orthogonal grids required that the SIMPLE algorithm be modified slightly to dampen numerical oscillations. A pressure-velocity coupling method for complex geometries, used by Ferziger and Perić [12], was implemented where an additional pressure-gradient term, as proposed by Rhie and Chow [21], was subtracted from the velocity value at the surface of the control volume to prevent non-physical oscillations. Several two-equation turbulence models and two sub-grid-scale (SGS) models were implemented for URANS and LES computations. In this study, LES and the γ-Re$_{\theta t}$ model – a correlation-based transition model [22], as implemented in [23] – were employed.

The calculations were performed mainly on moving grid configurations. The velocity of the grid movement and the gust velocity were included in the governing equations in an inertial frame of reference. It should be noted that the full flow velocity containing the gust component was used to calculate the diffusive terms for the momentum conservation in Eqs. (3) and (9), which was different from previous studies [9] and [10] where the gust velocity was neglected.

3. Computed Results and Discussion

In this study, the modified split-velocity method, combined with an RBF, was applied to model the gusting aerodynamics numerically and to investigate gust mitigation. The mitigation strategy is to use a pitch motion to reduce or change the effective angles of the wing when encountering gusts, as illustrated in Figure 1 for a pitching wing-gust encounter under a transverse gust.
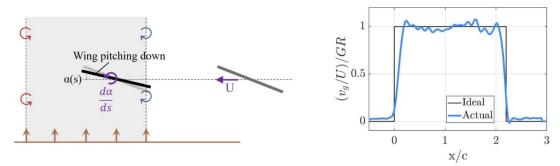

Figure 1 - Illustration of pitching wing-gust encounter; adopted from Andreu-Angulo & Babinsky [24].

3.1 Aerodynamic Response to Transverse Gust Encounters

Numerical simulations were performed for flat-plate wings undergoing transverse gust encounters. Sine-squared profiles were first considered in the numerical simulations. The flat-plate wing used by Biler et al. [10] in a water towing tank was selected as a test case. Detailed computations were discussed in [11].

The dimensions of the water tank were 7 m long, 1.5 m wide, and 1 m deep. The experimental gust system was designed to produce a spanwise planar gust of different velocities with a streamwise sine-squared profile. Transverse vertical gusts in the experiments were created by a variable speed water jet placed at the bottom of the water tank. Two thousand particle image velocimetry (PIV) images were acquired at 0.2 kHz, and mean velocity fields were obtained at 38.1 cm above the bottom of the water tank. A submergible ATI Mini-40 six-degree-of-freedom force balance was used to measure the forces and moments on the wing in a wing-fixed reference frame. The wing used in the experiments was a flat brass plate with a 5 cm chord, 20 cm span, and 0.03 thickness-to-chord ratio. Details of the experiment can be found in Biler et al. [10].

To reduce computational costs, only the half-span (10 cm) of the experimental rectangular wing was considered in the numerical simulations, and a symmetry boundary condition was specified at the

wing root (or mid-span of the experimental wing). The depth (height) of the computational domain was 1 m, the same as in the experimental measurements. The length was 2.1 m, ensuring a chord-wise distance of at least 20 chords from the wing to the boundaries in the streamwise direction, as shown in Figure 2. The width in the spanwise direction was set as 20 cm in the computational simulations, which is twice the semi-span of the wing.
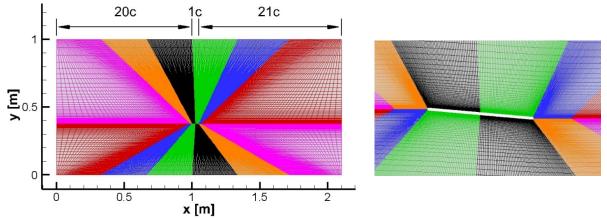

Figure 2 - Illustration of the computational domain and the mesh used for wing-gust interaction simulations.

Multi-block structured grids were used for the simulations, with two H-H type meshes attached to the wing upper and lower surfaces, two more as their extensions in the spanwise direction, and one O-H mesh filling the hole at the wing tip between the upper and lower extensions. The grid was generated using knowledge and experience gained from the computational work of reference [10]. Each H-H mesh had 441×97×33 grid points, with 161 points in the chord-wise direction on each surface of the wing, or 321 points in total on the whole surface of the wing and 97 points in the direction normal to the wall. These grids are slightly denser than those of the reference grid reported in the previous study [10], where 305 and 82 grid points were used, respectively. In the spanwise direction, our grid had 33 points along the half-span that was equivalent to 65 for an entire span, while 101 points were used along the span in the previous study [10]. However, the 3D LES simulations performed in this study showed identical integrated aerodynamic coefficients obtained from this proposed nominal grid compared to those from a refined grid that had 25% more grid points in all three directions. The grid was clustered at the wing surface. The wall grid spacing was set to $1 \times 10^{-4}c$, ensuring a resulting wall distance in wall units, y+, around a value of unity, the same as in the study of [10]. The O-H mesh filling the hole at the wing tip had 321×17×33 grid points. In the simulations, the five-block mesh was further decomposed into 25 partitions for parallel computing, as demonstrated in Figure 2.

Both LES and URANS (γ-Re$_{\theta t}$ model) simulations were carried out for a transverse vertical gust. In the simulations, the transverse gust had a streamwise sine-squared profile with a peak velocity of 0.13 m/s (or gust ratio GR = v_g/U = 0.16) and a width of 198 mm (4c). The angle of attack of the wing was set to 5 degrees. The simulations were carried out using a timestep $\Delta t = c/U/200$ with 60 pseudo-time steps. Halving the timestep Δt and doubling the pseudo-time steps did not improve the results. The computations were conducted for two setups. One used a moving body to mimic the experiment in the water towing tank and the other simulated the moving flow to mimic a wing impinged by a freestream, like in a wind tunnel. In the moving body configuration, the wing and the rigid mesh moved forward from right to left with a constant speed of 0.803 m/s while the gust did not move. In the configuration with a moving flow, the wing was stationary and the gust source moved together with the freestream from left to right at a velocity of 0.803 m/s. To allow moving-body simulations with a solid-body grid motion, a slippery wall boundary condition was applied to both the bottom and top sides. Figure 3 shows the computed results obtained for the moving body and moving flow configurations. The two sets of results overlapped at this flow condition. However, there were differences between the LES and URANS results, particularly in the pitching moment, which is not shown here but can be found in [11]. The pitching moment is critical for predicting aeroelastic effects

and flight stability correctly. The URANS simulation was performed using the γ-Re$_{\theta t}$ turbulence model [22], which contains a transition model.

As shown in Figure 3, the leading edge of the wing entered the gust at UΔt/c = 0 and the trailing edge left the gust at UΔt/c = 5. The predicted lift coefficients showed a peak value in accordance with the gust peak at UΔt/c = 2.5. All four simulations using the LES and URANS methods on both the moving-body and moving-flow configurations predicted the same lift peak, because this lift peak was mainly driven by the vertical gust. The computations showed a discrepancy of about 10% for the lift coefficient when compared with the experimental data. Considering the high fluctuations of the gust velocity with a standard deviation of 30% of the mean gust velocity and a ~14% error bar for the mean peak velocity in the experiment [10], the computed lift coefficient is believed to be close to or even within the measurement error bar. There was a timing difference in the lift coefficients between the CFD and experiment, which is believed to be caused by the deviation of the gust profiles in the region through which the wing passed. The imposed gust in the CFD simulations had an exact symmetrical sine-squared profile, whereas setting the pump inlet at the left side in [10] might have caused a slight chordwise flow from right to left in the experiment. This right-to-left motion of the fluid in the water tank could slightly delay the wing entering the peak of the gust, resulting in the occurrence of the experimental peak lift slightly after UΔt/c = 2.5. In addition, the lift dip that was experimentally observed while the wing entered the gust was not captured in the current CFD analysis. This was attributed to the fact that there exist deviations between the computational and experimental conditions. In the numerical simulations, the introduced gust profile was nearly accurate for the location through which the wing passed, but it did not exactly match the jet inflow at the bottom of the water tank in the experiment.
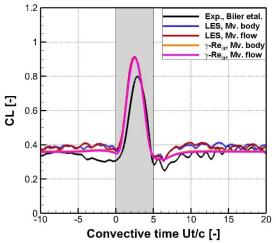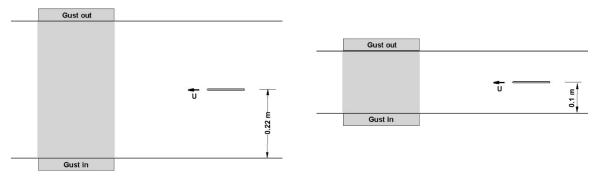

Figure 3 - Lift coefficients for the flat-plate wing past the transverse sine-squared gust at α = 5° and GR = 0.16.

The lift responses to the sine-squared gust at different angles of attack and at similar peak effective angles of attack were investigated in [11]. As expected, the lift force increased with the angle of attack. The computations at similar peak effective angles of attack predicted peak forces that were close, but not exactly the same, because the effective angles were close at the leading edge but different along the chord length.

3.2 Gust Generator Outlet Location Effects

The developed code was used to investigate the effects of the distance between the test wing and the outlet of the gust generator. A test case using the top-hat gust profile from Andreu-Angulo & Babinsky [24] was selected as a reference. The wing model used in the experiment consisted of a glass plate with a chord length of 0.12 m, a span of 0.48 m, a thickness of 0.004 m, and rounded leading and trailing edges. These dimensions of the wing were kept the same in the present numerical simulations.

Andreu-Angulo & Babinsky [25] and [26] discussed their experimental results mainly when the wing was located 0.1 m away from the gust generator outlet. In the same water towing tank at the University of Cambridge, earlier experimental measurements [27] and a more recent one [28] were conducted with the wing placed 0.22 m from the gust outlet. Figure 4 illustrates the two configurations used in this computational study, where the outlet of the gust generator is assumed to be located at the bottom of the computational domain marked as "gust in" in the computations.

<table>
<tr><td>a) 0.22 m case</td><td>b) 0.1 m case</td></tr>
</table>

Figure 4 – Computational configurations based on experimental setups used by Andreu-Angulo & Babinsky [24] – [26], [28].

In this study, the wing traveled at a constant velocity from right to left with a resulting Reynolds number of 30,000 through an ideal sharp-edged top-hat gust profile shown in Figure 1. The gust ratio (GR) was equal to 1, and the gust had a width of two chord lengths or 0.24 m [25]. The grid size was similar to the one used in the earlier wing-gust interactions with the sine-squared gusts.

The measurements showed deviations of the lift forces. Figure 5 compares the lift forces, confirming that the distance from the wing to the gust generator affected the lift force; the closer the wing is to the gust generator outlet, the higher is the generated lift. Figure 6 shows the pressure distribution on the cross-section at the mid-span (middle between the wing root and tip) of the wing. When compared against the left plot of the 0.22 m configuration, a larger suction zone on the upper surface of the wing was clearly visible in the right plot for the 0.1 m case, resulting in a higher lift force. Note that the pressure distribution was defined based on the freestream velocity. Because of the gust effects, the peak of the pressure distributions was higher than one and close to two in this case. Figure 7 further compares the surface pressure. As indicated by the curves, the integrated lift of the 0.1 m case was visibly higher than that of the 0.22 m case.
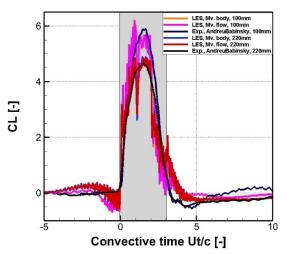

Figure 5 - Lift responses of the pitching wing to a sharp-edged top-hat gust when the wing is located at one of two distances from the gust generator outlet; experimental data supplied by Andreu-Angulo & Babinsky [28].
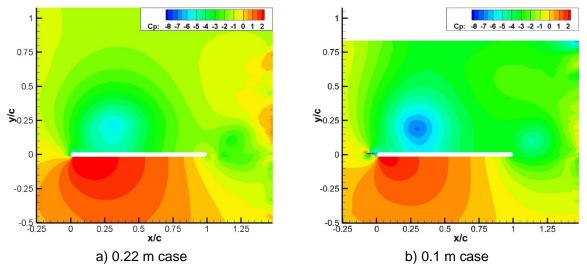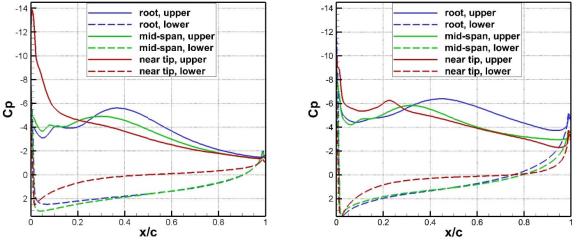
a) 0.22 m case b) 0.1 m case

Figure 6 - Computed pressure distribution on the cross-section at the mid-span of the wing at two distances from the gust generator outlet when the wing entered the center of the gust.

a) 0.22 m case b) 0.1 m case

Figure 7 - Computed surface pressure on the wing at two distances from the gust generator outlet when the wing entered the center of the gust.

3.3 Numerical Modelling of Mitigation of Gust Effects

The developed code was also applied to simulate gust mitigation of a sharp-edged top-hat gust. In this study, the simulations were mainly focused on the configuration with a distance of 0.22 m, to minimize possible interference with the bottom wall at the gust inlet of the computational domain. Figure 8 compares the computed lift coefficient with the experimental data from Andreu-Angulo & Babinsky [28]. The numerical simulations were first performed for the case with no mitigation technique applied. The pitching profile used by Andreu-Angulo & Babinsky for the experiments in their water towing tank [28] was supplied as input in the numerical simulations. For the case where a mitigation technique was applied, the current CFD simulations predicted a peak lift force comparable to the experimental data. Also, they correctly captured the force dip prior to entering the gust. When the pitching mitigation was applied, the lift force was significantly reduced. However, the numerical simulations showed large oscillations, which needs to be confirmed as the experimental data were presented after filtering. Figure 9 and Figure 10 compare the pressure distributions when the wing entered the center of the gust. As shown in Figure 9 and Figure 10, the pitch motion reduced the pressure difference between the upper and lower surfaces significantly, thus reducing the lift.
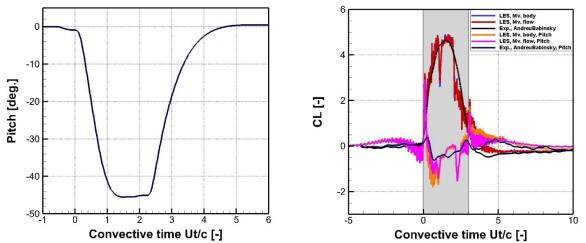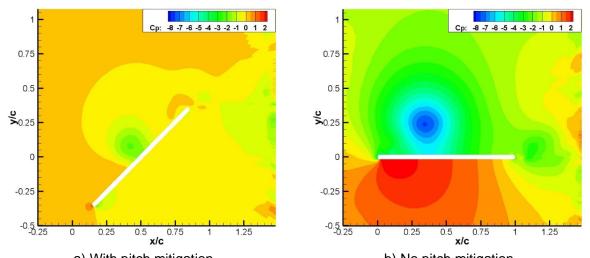
Figure 8 - Pitching profile and lift response of a pitching wing to sharp-edged top-hat gust; pitching profile and measured lift coefficients provided by Andreu-Angulo & Babinsky [28].

a) With pitch mitigation   b) No pitch mitigation

Figure 9 - Computed pressure distribution on the cross-sections at the root of the wing located 0.22 m from the gust generator outlet when the wing entered into the center of the gust.

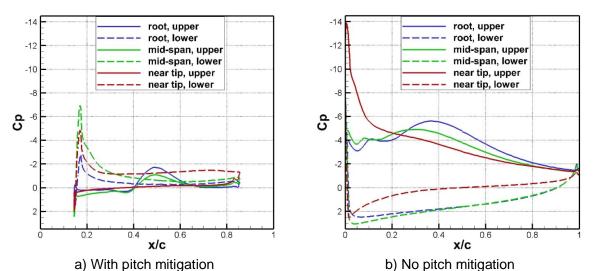a) With pitch mitigation   b) No pitch mitigation

Figure 10 - Computed surface pressure on the wing located 0.22 m from the gust generator outlet when the pitching wing entered the center of the gust.

4. Concluding Remarks

The split-velocity method, originally proposed by Wales et al. [8] for compressible flows, was further developed for gust modelling in incompressible flow regimes. Towards real-world applications, the split-velocity method was extended from the 2D Euler to the 3D Navier-Stokes equations. The conservative form of the equations was employed for the gust source terms in this study, which is different from the original method [8]. This maintains consistency in the discretization of both the gust and the remaining velocity of the flow, improving the momentum conservation and numerical stability. The gust velocity was included in the discretization of the viscous terms to ensure the accuracy of the predicted flow physics because the gust is a part of the flow, whereas the gust velocity was neglected in [9] and [10]. Furthermore, while the split-velocity method was originally designed for stationary configurations, it was extended to moving configurations in this study. However, the present study did not include the gust velocity in the grid velocity to ensure strict mass conservation in the space conservation law of simulations on moving grids, whereas it was included in the previous studies using field-velocity methods [6] and [7].

The RBF technique was implemented and applied to the modified split-velocity method, allowing simulations of gust mitigation using flexible or morphing wings. The computed results showed lift reduction comparable to experimental data when the pitching motion was applied as a gust mitigation technique.

The numerical techniques built a necessary foundation to tackle more challenging problems for real-world UAV applications in urban environment. Further improvements of the techniques will support the applications, including developing a more accurate discretization scheme for gust modelling on computational domain boundaries allowing the grid points on the boundaries to represent better the gust distribution while further validating using experimental data being acquired at a wind tunnel at RMC.

5. Acknowledgments

6. Contact Author Email Address

Weixing.Yuan@nrc-cnrc.gc.ca

7. Copyright Statement

References

[1] Theodore, C., Tischler, M., and Colbourne, J. Rapid Frequency-Domain Modelling Methods for Unmanned Aerial Vehicle Flight Control Applications. *Journal of Aircraft*, Vol. 41, No. 4, 2004.

[2] Etele, J. *Overview of Wind Gust Modelling with Application to Autonomous Low-Level UAV Control.* DRDC Ottawa CR 2006-221, 2006.

[3] Poirel D., and Price, P. Structurally Nonlinear Fluttering Airfoil in Turbulent Flow. *AIAA Journal*, Vol. 39, No. 10, 2001.

[4] Lockard, D., and Morris, P. Radiated Noise from Airfoils in Realistic Mean Flows. *AIAA Journal*, Vol. 36, No. 6, 1998.

[5] Golubev, V., Dreyer, B., Golubev, N., and Visbal, M. High-Accuracy Viscous Simulations of Gust Interaction with Stationary and Pitching Wing Sections. *47th AIAA Aerospace Sciences Meeting Including The New Horizons Forum and Aerospace Exposition*, 5 - 8 January 2009, Orlando, AIAA 2009-11.

[6] Singh, R., and Baeder, J. D. Direct Calculation of Three-Dimensional Indicial Lift Response Using Computational Fluid Dynamics. *Journal of Aircraft*, Vol. 34, No. 4, 1997, pp. 465–471.

[7] Sitaraman, J., and Baeder, J. D. Field Velocity Approach and Geometric Conservation Law for Unsteady Flow Simulations. *AIAA Journal*, Vol. 44, No. 9, 2006, pp. 2084–2094.

[8] Wales, C., Jones, D., and Gaitonde, A. Prescribed Velocity Method for Simulation of Aerofoil Gust

Responses. *Journal of Aircraft*, Vol. 52, No. 1, 2014, pp. 64–76. doi:10.2514/1.C032597.

[9] Badrya, C., Baeder, J., Jones, A. Application of Prescribed Velocity Methods to a Large-Amplitude Flat-Plate Gust Encounter. *AIAA Journal*, Vol. 57, No. 8, 2019, pp. 1960-1968.

[10] Biler, H., Badrya, C., Jones, R. Experimental and Computational Investigation of Transverse Gust Encounters. *AIAA Journal*, Vol. 57, No. 11, 2019. DOI: 10.2514/1.J057646.

[11] Yuan, W., Zhang, X., and Poirel, D. Numerical Modelling of Aerodynamic Response to Gust. *AIAA SciTech Forum*, Virtual Event, 11-15 & 19-21 January 2021, AIAA 2021-2001.

[12] Ferziger, J. H., and Perić, M. *Computational Methods for Fluid Dynamics*. Springer-Verlag, Berlin & Heidelberg, 1996.

[13] Demirdžić, I., and Perić, M. Finite Volume Method for Prediction of Fluid Flow in Arbitrarily Shaped Domains with Moving Boundaries. *International Journal for Numerical Methods in Fluids*, Vol. 10, pp. 771-790, 1990.

[14] Cella, U., and Biancolini, M. Aeroelastic Aanalysis of Aircraft Wind-Tunnel Model Coupling Structural and Fluid Dynamic Codes. *J. of Aircraft*, Vol. 49, No. 2, pp. 407-414, 2012.

[15] Yuan, W., Sandhu, R., and Poirel, D. Fully Coupled Aeroelastic Analyses of Wing Flutter towards Application to Complex Aircraft Configurations. Journal of Aerospace Engineering, 34(2), 2021.

[16] Yuan, W., and Khalid, M. Computation of Unsteady Flows past Aircraft Wings at Low Reynolds Numbers. *Canadian Aeronautics and Space Journal*, 50(4): 261-271, 2004.

[17] Yuan, W., Khalid, M., Windte, J., Scholz, U., and Radespiel, R. Computational and Experimental Investigations of Low-Reynolds-Number Flows past an Airfoil. *The Aeronautical Journal*, 111(1115):17-29, 2007.

[18] Yuan, W., Lee, R., Hoogkamp, E., Khalid, M. Numerical and Experimental Simulations of Flapping Wings. *International Journal of Micro Air Vehicle*, Vol. 2, No. 3, pp. 181-209, 2010.

[19] Yuan, W., Poirel, D., Wang, B. Simulations of Pitch-heave Limit-cycle Oscillations at a Transitional Reynolds Number. *AIAA Journal*, Vol. 51, No. 7, pp. 1716-1732, 2013. DOI: 10.2514/1.J052225.

[20] Patankar, S. V. *Numerical Heat Transfer and Fluid Flow*. Hemisphere Publishing Corporation, Washington, 1980.

[21] Rhie, C. M. and Chow, W. L. Numerical Study of the Turbulent Flow past an Airfoil with Trailing Edge Separation. *AIAA Journal*, Vol. 21, No. 11, pp. 1525-1532, 1983.

[22] Langtry, R. and Menter, F. Correlation-Based Transition Modelling for Unstructured Parallelized Computational Fluid Dynamics Codes. *AIAA Journal*, 47(12):2894-2906, 2009.

[23] Yuan, W., Poirel, D., Wang, B., Benaissa, A. Effect of Freestream Turbulence on Airfoil Limit-Cycle Oscillations at Transitional Reynolds Numbers. *AIAA Journal of Aircraft*, Vol. 52, No. 4, pp. 1214-1225, 2015. doi: http://arc.aiaa.org/doi/abs/10.2514/1.C032807.

[24] Andreu-Angulo, I. and Babinsky, H. Controlling Upwards and Downwards Gust Loads on Aerofoils by Pitching. *AIAA SciTech Forum*, 3-7 January 2022, San Diego, CA, AIAA 2022-0332.

[25] Andreu-Angulo, I. and Babinsky, H. Unsteady Modelling of Pitching Wings for Gust Mitigation. *AIAA SciTech Forum*, Virtual Event, 11-15 & 19-21 January 2021, AIAA 2021-1999.

[26] Andreu-Angulo, I. and Babinsky, H. Negating Gust Effects by Actively Pitching a Wing. *AIAA SciTech Forum*, 6-10 January 2020, Orlando, FL, AIAA 2020-1057.

[27] Corkery, S., Babinsky, H., and Harvey, J. On the Development and Early Observations from a Towing Tank-based Transverse Wing–gust Encounter Test Rig. *Experiments in Fluids*, Vol. 59, No. 135, 2015. https://doi.org/10.1007/s00348-018-2586-0.

[28] Andreu-Angulo, I. and Babinsky, H. Mitigation of Aerofoil Gust Loads through Pitch. Accepted for *AIAA Journal*, 2022.